JTTEE5 10:382-389

Modeling and Visualization of Plasma Spraying of Functionally Graded Materials and Its Application to the Optimization of Spray Conditions

Y. P. Wan, V. Gupta, Q. Deng, S. Sampath, V. Prasad, R. Williamson, and J. R. Fincke

(Submitted 8 February 2000; in revised form 9 November 2000)

This paper presents a simulation and visualization system for plasma spraying of functionally graded materials (FGM). The recently modified CFD code, LAVA-P, that incorporates a well-verified model for plasma gas flow and chemistry is employed. The particle movement and its trajectory are described within a Lagrangian formulation by considering drag as the major driving force, and the particle melting, evaporation, and resolidification are considered using a recently developed model for particle-flame interaction. In addition to the noncontinuum and variable property effects associated with high-temperature plasma, the effects of particle evaporation on particle momentum and heat transfer are also taken into account. Calculations are performed for NiCrAlY and ZrO_2 powders for a wide range of size distributions. The influences of power levels and flow rate of H_2 on plasma flow field and, hence, on the particle velocity and temperature are investigated. The predicted velocity and temperature fields agree well with the measurements under similar spraying conditions. With the help of a special in-house built process animation and visualization algorithm, the powder injection conditions, such as the number of injectors, injector location, and injection velocity, are investigated and can be optimized to obtain coatings with a specified distribution of different species.

Keywords: modeling, FGM, plasma spray

1. Introduction

Plasma spraying has emerged as a practical method to produce the coatings of functionally graded materials (FGMs), in which powders of two or more materials are injected at varying rates into a high-temperature plasma jet. These particles after being heated and accelerated impact a substrate to form a coating that has either continuously or stepwise varying compositions and/or microstructures. One of the major objectives in the fabrication of FGMs is that the final structure should vary in a desired regular and consistent manner. Since the thermophysical properties (*e.g.*, melting temperature and density) of powder materials can vary greatly, attempts to produce desired FGMs involve laborious trial and error experiments to determine the precise spray parameters for each kind of graded coating. The process parameters, such as the power level, the flow rate of primary and secondary gases, the powder injector configuration, *etc.*, consist of so many possible combinations that this "Edisonian" type optimization process consumes an immense amount of time and resources to develop a repeatable process for desired coatings. Therefore, it is important that the relationship between the gun operating parameters and the resulting particle trajectories and temperatures, *etc.*, is well understood and predictable.

For this purpose, a series of experiments[1–3] has been carried out using a Metco-9MB DC plasma spray system at the Idaho National Engineering and Environment Laboratory. These measurements provide a comprehensive database for velocity and temperature of different kinds of particles under varying conditions of the current, voltage, and hydrogen flow rate.

Segregation patterns of powder species on the deposition reported in Ref 3 show the necessary control of particle trajectories through the configurations of powder injectors.

The primary goal of this work is to develop a reliable model for the simulation of plasma spraying of FGMs, use of which can minimize the tedious and expensive trial and error optimization experiments. The detailed mathematical models for plasma flow and particle movement have been described in another publication;[4] the focus here is on the validation of the complete model by comparing the calculations with experimental results, and development of an animation and visualization algorithm.

2. Physics-Based Computer Model

In our model, the argon-hydrogen plasma jet is simulated using the LAVA code,[5] which is a three-dimensional CFD software developed for transient simulations of thermal plasma. The comprehensive mathematical formulation employed in this algorithm treats the plasma as a compressible, multicomponent, chemically reacting ideal gas with temperature-dependent ther-

Y. P. Wan, V. Gupta, Q. Deng, S. Sampath, and **V. Prasad,** Center for Thermal Spray Research and Process Modeling Laboratory, State University of New York at Stony Brook, Stony Brook, NY 11794-2275; and **R. Williamson** and **J. R. Fincke,** Idaho National Engineering and Environment Laboratory, ID 83415-2211. Contact e-mail: yuepeng.wan@sunysb.edu.

mophysical and transport properties. Ionization, dissociation, recombination, and other chemical reactions are treated using a general kinetic algorithm.[6] A reduced set of reactions[6,7] is used for the Ar-H_2 plasma considered here. A detailed description of the physical model and numerical techniques incorporated into LAVA can be found in the article by Ramshaw and Chang.[5]

LAVA solves the convection-diffusion transport equations, whose general form for a two-dimensional cylindrical coordinate system is given as

$$\frac{\partial(\bar{\rho}\tilde{\varphi})}{\partial t}+\frac{1}{r}\frac{\partial(\bar{\rho}r\tilde{u}\tilde{\varphi})}{\partial r}+\frac{\partial(\bar{\rho}\tilde{v}\tilde{\varphi})}{\partial y}=\frac{1}{r}\frac{\partial}{\partial r}\left(\frac{\mu+\mu_t}{\sigma_{\tilde{\varphi}}}r\frac{\partial\tilde{\varphi}}{\partial r}\right)+\frac{\partial}{\partial y}\left(\frac{\mu+\mu_t}{\sigma_{\tilde{\varphi}}}\frac{\partial\tilde{\varphi}}{\partial y}\right)+S_{\tilde{\varphi}} \quad \text{(Eq 1)}$$

Here, $\tilde{\varphi}$ represents all the Favre-averaged dependent variables, including velocities in r and y directions, $\tilde{u}$ and $\tilde{v}$ and represent the mass fraction of chemical species and thermal energy. In Eq 1, S_φ is a general representation of the source term for variable $\tilde{\varphi}$. The standard $\tilde{k}-\tilde{\varepsilon}$ model[8] is used to estimate the turbulent viscosity μ_t and the equations for $\tilde{k}$ and $\tilde{\varepsilon}$ follow the general form of Eq 1. Local thermodynamic equilibrium is assumed within the plasma jet for the calculations reported here.

The plasma gas flow is considered to be without any swirl, and the influence of the carrier gas on plasma flow field is ignored. The reasons for ignoring the carrier gas effect are as follows. (1) The carrier gas flow rate is 5 slm, relatively very low compared to the flow rate of primary and secondary plasma gas, which is about 52 slm. (2) The carrier gas can cause the plasma flow to be asymmetric; hence, requiring time-consuming three-dimensional calculations.

An algorithm for thermal interaction between the plasma and powder particles has been added to LAVA, and this new version of LAVA, which is able to handle multiple particles and can account for particle heating, melting, evaporation, and resolidification, is called LAVA-P.[4] In this model, the injected powder particles are discretely treated in a Lagrangian manner. The particles (particle groups, in fact) are introduced at the point of injection and tracked throughout their flight. Spherical symmetry is assumed to be applicable to powder particles, and internal convection within the molten part of the particle is considered negligible. The particle is heated (or cooled) by surrounding plasma gas through heat convection and thermal radiation. The temperature distribution within the particle is governed by internal heat conduction. The conduction equation is solved by tracking the movement of solid-melt interface and the change in the outer boundary of the particle due to evaporation. Effects on convective heat transfer due to variable plasma properties,[9] noncontinuum properties of the plasma gas,[10] and mass transfer due to evaporation[4] are also taken into consideration. A detailed description of this model for particle heating, melting, resolidification, and evaporation, and the solution method for moving interfaces and boundaries, can be found in Ref 4.

Drag is considered to be the dominating driving force for the momentum exchange. Also, the effects of variable plasma properties and the Knudsen noncontinuum effect on the driving force are included in the present model. A nonuniform mesh of 56 grids in the x direction and 65 grids in the y direction is selected for the plasma gas calculations performed here.

Table 1 Processing parameters for the benchmark case

Processing parameter	Value
Current	500 A
Voltage	70 V
Power efficiency	0.7
Primary gas flow	40 slm Ar
Secondary gas flow	12 slm H_2
Feed rate	4 rpm

Table 2 Operating conditions for the cases calculated

	Currency (A)	Voltage (V)	H_2 (slm)
Ca400A	400	70	12
Ca450A	450	70	12
Ca550A	550	70	12
Ca600A	600	70	12
CaH0	500	32.3	0
CaH2	500	50	2
CaH4	500	55	4
CaH6	500	59.5	6
CaH8	500	63	8
CaH10	500	67.5	10
Benchmark	500	70	12

The goal of our visualization system is to provide a better visual understanding of the effects of changes in various parameters, such as nozzle location, injection velocity, plasma conditions, and different particle properties including their size.

The visualization algorithm for the time-varying thermal spray deposition process has been written in C and OpenGL, and runs on a SGI Onyx 2. Some example screen shots of this system appear in Fig. 8 to 11. The details of the technique employed in this visualization system have been described in a previous paper.[11]

3. Process Conditions for Simulation

The present study has been conducted for atmospheric plasma spray of a commercial Metco 9MB plasma gun.[2] The processing conditions used for the calculations reported here are selected from that reported in the experiments of Smith *et al*.[2] The detailed operating conditions for the benchmark case are listed in Table 1. For other cases, either the arc current intensity or the flow rate of H_2 (and, correspondingly, the arc voltage) is different from the benchmark case, and the corresponding conditions are listed in Table 2. The nozzle diameter of the plasma gun is 7.5 mm and the powder is fed with the carrier gas of argon from outside the plasma gun, as illustrated in Fig. 1. The powder port is located axially 6.0 mm downstream from the nozzle exit and vertically 8.0 mm above the axis of the nozzle. The internal diameter of the powder injector is 1.25 mm.

For cases to be compared to the experimental data, partially stabilized zirconia (ZrO_2) and NiCrAlY powders are injected separately from the same injector with different injection velocities, 14.5 m/s for ZrO_2 particles and 9.8 m/s for NiCrAlY particles, as listed in Table 4. For the species segregation calculations, different injector configurations are used whose conditions are described later. The particle sizes used in the calculations correspond to PSZ2 and NiCrAlY2 as in Ref 2 and are

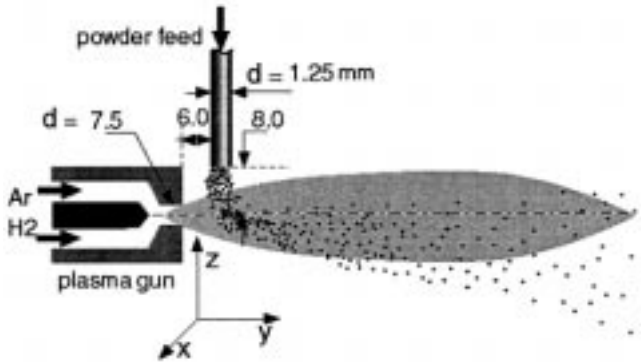

Fig. 1 Illustration of the plasma spray system being simulated

Table 3 Powder characteristics

Powder species	Particle size range (μm)	Average size (μm)	Morphology	Density (g/cm^3)
NiCrAlY	43 to 91	62	Spherical	8.11
ZrO_2	30 to 99	58	Spherical	5.89

listed in Table 3. A flat size distribution for both powder species is assumed here for simplicity, although the model is capable of employing any size distribution.

The thermodynamic properties of ZrO_2 are taken from Samsonov.[12] Thermal properties of NiCrAlY are not well known and cannot be found in the literature. We use the thermal conductivity, heat capacity, melting point, and evaporation properties of pure nickel to represent that of NiCrAlY. This may cause inaccuracy in the predictions of temperature for NiCrAlY particles, as displayed in Fig. 4(b) and 5(b). The thermodynamic properties of nickel are selected from Hultgren *et al*.[13]

The calculation was first run 5 ms to steady state in the absence of particles. The resulting plasma solutions served as the initial conditions for transient simulations of the particle behavior.

4. Results and Discussions

Simulation results for the process conditions described in Section 3 are presented here.

4.1 Gas Velocity and Temperature at the Nozzle Exit

The velocity and temperature of plasma gas at the nozzle exit are determined directly from the operating conditions. They are correlated to the arc voltage, currency intensity, and flow rates of primary and secondary gases through mass balance and energy balance.[5] In the calculation, the velocity and temperature profiles at the exit have to be provided as boundary conditions. The following expressions[5] are used for plasma velocity and temperature profiles at the exit:

$$v = v_0\left[1-\left(\frac{r}{R_0}\right)^{n_v}\right];\ \frac{T-T_\infty}{T_0-T_\infty}=\left[1-\left(\frac{r}{R_0}\right)^{n_T}\right] \qquad \text{(Eq 2)}$$

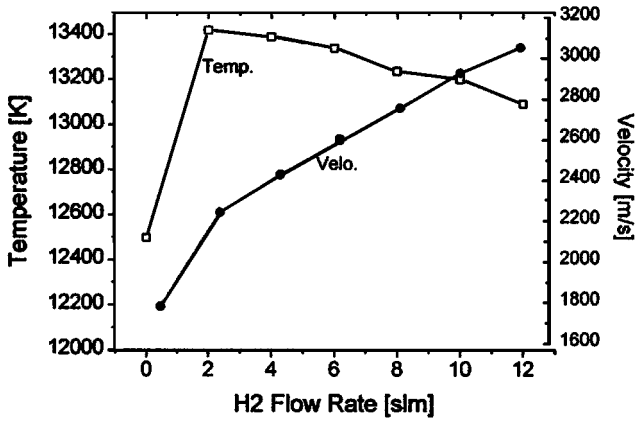

Fig. 2 Plasma gas velocity and temperature at the centerline of the exit for the cases with different hydrogen flow rates

Table 4 Powder particle injection velocity[1]

	NiCrAlY (m/s)	ZrO_2 (m/s)
Separate injection	9.8	14.5
Mixed injection	11.7	11.7
Two injectors	9.8	14.5
Two injectors, same velocity	11.7	11.7

where v_0 and T_0 are velocity and temperature at the centerline of the nozzle exit, respectively, whose values are determined by the spraying conditions. The term T_∞ is the ambient temperature. The value of the power indices n_v and n_T have to be fixed by comparing the calculated v_0 and T_0 with the experimental data. The values of 1.2 and 6.0, respectively, are found to be appropriate for the present cases. For the cases with different hydrogen flow rates, the velocity and temperature at the exit centerline are plotted in Fig. 2. Generally, the velocity increases as the flow rate of hydrogen becomes larger, and the temperature drops slightly except for the case of zero hydrogen flow rate. The exceptional low temperature in this case is because of the very low voltage (32.5 V) associated with zero hydrogen flow rate. For the hydrogen flow rates considered here, the variation of temperature is less than 10%, while the variation of velocity is more than 40%. Evidently, the flow rate of hydrogen has more influence on the velocity than on the temperature of the plasma jet.

4.2 Particle Velocity and Temperature History

Before we attempt to compare the calculations with the measurements, it is necessary to re-examine the methods used in the measurements of Smith *et al*.[2] and to interpret the experimental data appropriately, so that the comparison makes sense. In the experiments of Smith *et al.*, the transverse and axial particle trajectory patterns were obtained with a spray pattern trajectory (SPT) sensor. In addition, a laser doppler velocimetry system capable of spectral width measurements was used to measure the average velocity and size of the particles. For the measurement of the particle velocity along the axis, as shown in Fig. 3(a), 4(a), 5(a), and 6(a), the SPT sensor was focused on a very small region near the axis. Therefore, the averaged axial velocity of particles is actually the velocity of

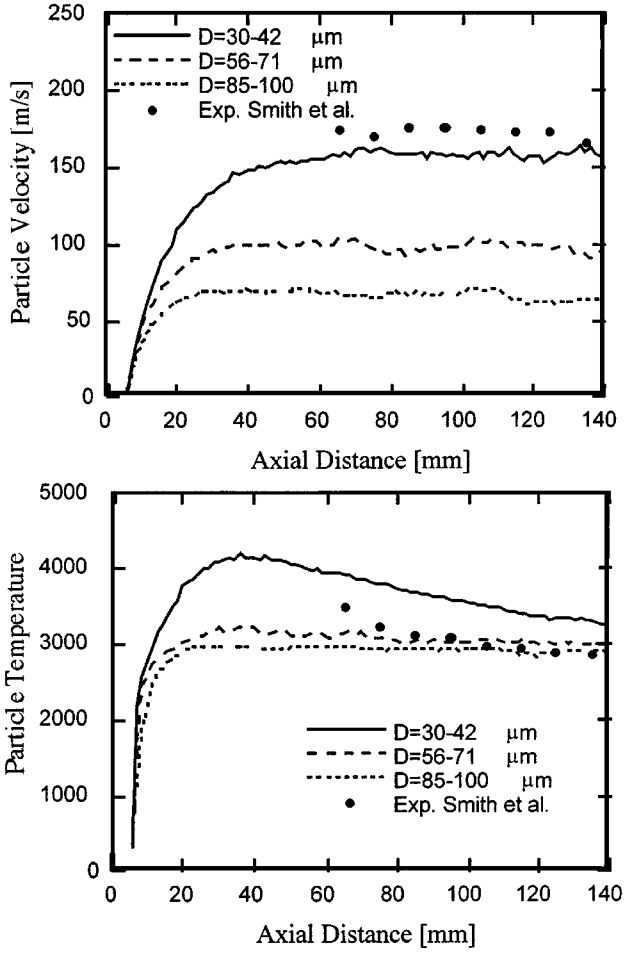

Fig. 3 Axial velocity and temperature of ZrO_2 particles with different sizes along the axial distance. Experimental data of Smith *et al.*[2] are plotted as a reference

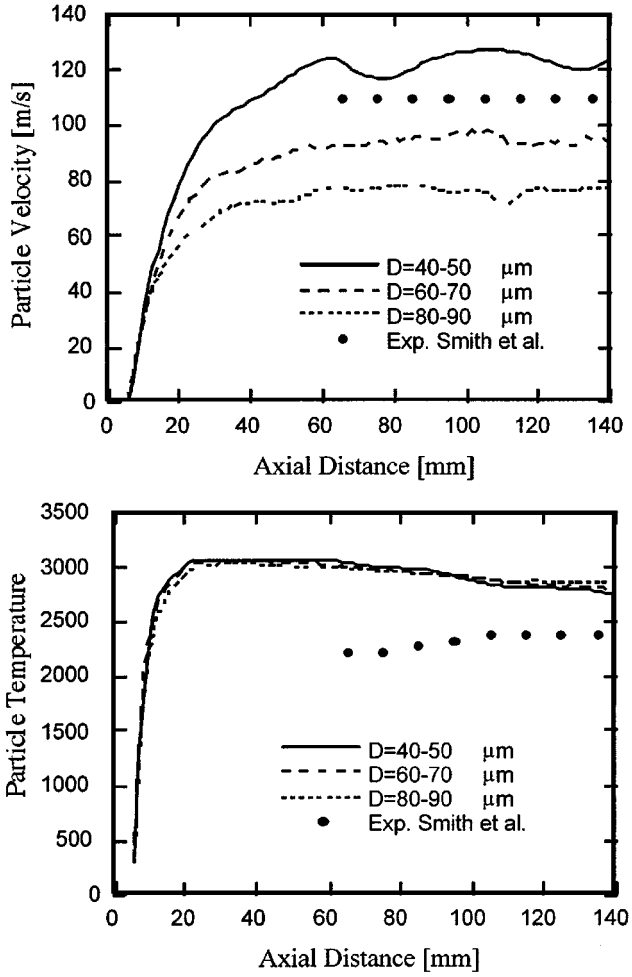

Fig. 4 Axial velocity and temperature of NiCrAlY particles with different sizes along the axial distance. Experimental data of Smith *et al.*[2] are plotted as a reference

those particles that are traveling in a narrow zone along the axis. These are mostly the particles with small sizes, since the large particles move away to the periphery of the flame due to their larger inertia. The average in-flight particle temperature was determined using a two-color pyrometer, IPP2000. Obviously, the measured particle temperature was an averaged temperature of many of the particles moving through the focused window.

Results shown in Fig. 3 and 4 are the particle velocity and temperature along the central axis for the benchmark case. The calculated data are number-averaged values for the particles with the size in a specified size group; Three size groups are presented. Two other size groups in between are not shown in these figures. Both Fig. 3(a) and 4(a) show that smaller particles have much higher axial velocity than the larger ones. The difference in velocity between the larger and smaller groups can be over 30% for NiCrAlY particles (Fig. 4a) and even greater than 50% for ZrO_2 particles (Fig. 3a). The larger variation of velocity in the case of ZrO_2 particles is because of the larger size difference. The reason for smaller particles having larger velocities is that smaller particles can be easily accelerated by the surrounding plasma gas. For the same reason, the flight time of a smaller particle in the flame is shorter than that of the larger one, and therefore, since most of the particles traverse along the axis of the plasma plume, the positions of smaller particles are closer to the axis than the larger ones. Since the signals collected in the experiments of Smith *et al.*[2] using an SPT sensor focusing on the axis come mostly from the particles with smaller sizes, the experimental data plotted in Fig. 3(a) and 4(a) represent the velocity of the particles in the smallest size group. In this sense, the agreement between the predictions and the measurements shown in both figures is quite good. The slightly higher velocity of ZrO_2 particles is attributed to its lower density compared to that of the NiCrAlY particles.

The calculated number-averaged temperature of the ZrO_2 particles is in reasonable agreement with the measurements, as shown in Fig. 3(b). While the smaller particles display much larger overheating, the large size particles just reach the melting point (2950 K) with many of them only partially melted or not even melted. This is because the larger particles have much higher total heat capacity and need more time to be heated; moreover, the general trajectories of large particles are further

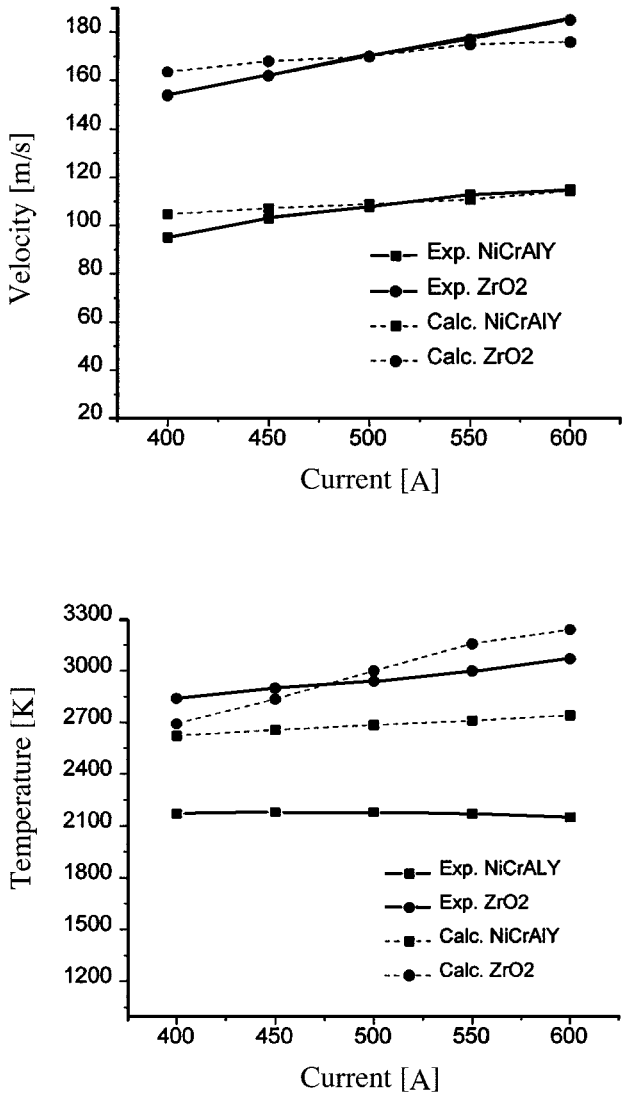

Fig. 5 Comparison of calculated average velocity and temperature of ZrO_2 and NiCrAlY particles at the axial distance of 100 mm for different current levels, compared with the experimental data of Smith *et al.*[2]

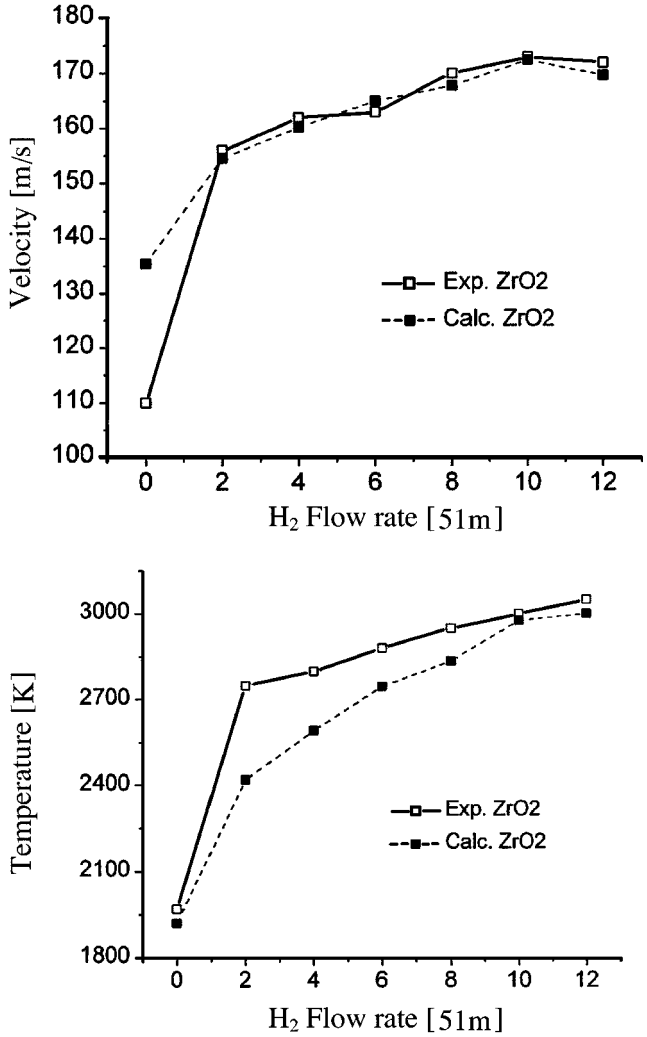

Fig. 6 Comparison of calculated velocity and temperature of ZrO_2 particles at the axial distance of 100 mm for the cases with different hydrogen flow rates with the experimental data of Smith *et al.*[2]

away from the hot core of the flame. Figure 3(b) also shows that the smaller particles cool rapidly while the larger particles keep their temperature around the melting point during the flight.

The results on the temperature of NiCrAlY particles are plotted in Fig. 4(b). As mentioned before, the thermal properties used in the calculation are that of the nickel instead of NiCrAlY. We are not attempting to compare the results with the experimental data for NiCrAlY, although we also show these data on the same plot just as a reference. In Fig. 4(b), we see no great difference in the temperature between the particles with difference sizes. The main reason is the low boiling point (3100 K) of nickel, which is the maximum temperature the particle can reach. Most of the nickel particles get heated to the boiling point and start vaporizing. The temperature begins to drop when the surrounding plasma gas temperature decreases, and eventually, the smaller particles reach slightly lower temperatures.

Figure 8 is a snapshot of the animated spray, in which the temperature field of both plasma gas and powder particles (here, PSZ particles) are demonstrated with a color map. (The image on the upper-right corner shows the growth of a coating layer). The physical size of particles is represented by the size of the flying circles on the screen.

4.3 Particle Velocity and Temperature with the Variation of Current

The numerical results shown in both Fig. 5 and 6 are the number-averaged velocity and temperature of the particles that are passing through the axial position of 100 mm. The collection window for particle velocity is from 0 to −10 mm in the *z* direction; refer to Fig. 1, which closely represents the focused region of the SPT sensor in the measurements. To calculate the particle temperature, all particles flying through the *x*–*z* plane at an axial distance of 100 mm are taken into averaging.

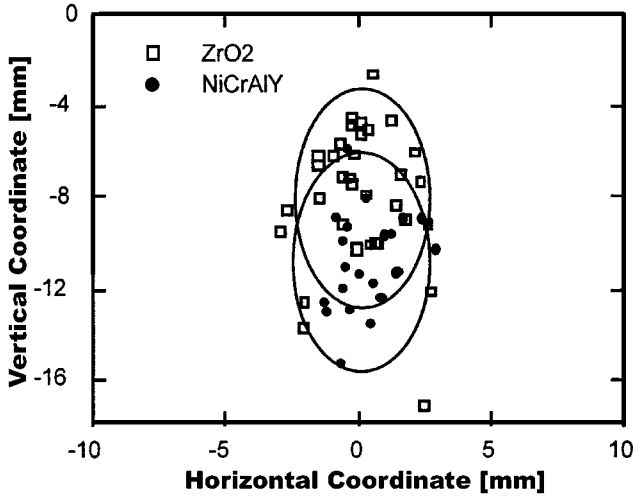

(a)

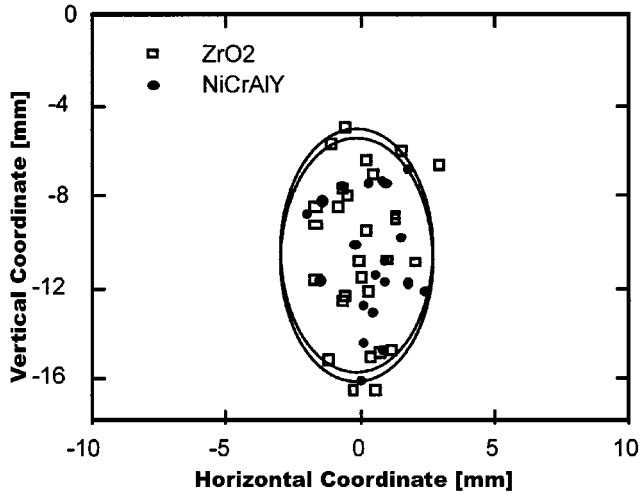

(b)

Fig. 7 Calculated deposition positions of both ZrO2 and NiCrAlY particles on the plane at the axial distance of 100 mm. (**a**) Both materials are injected together through the same injector. (**b**) Two injectors with the same injection velocity (11.7 m/s)

As shown in Fig. 5, the results for both ZrO_2 and NiCrAlY particles agree well with the measurement data, except the temperature of NiCrAlY due to the use of the thermophysical properties of nickel. The NiCrAlY particles have generally lower velocities than the ZrO_2 particles because of the higher density of NiCrAlY (Fig. 5a). The temperature of NiCrAlY is much lower than that of ZrO_2 (Fig. 5b). The reason is that NiCrAlY has a much lower boiling point and the temperatures of these particles at this standoff are very close to the boiling point.

For both materials, the particle velocity increases with the current value, as shown in Fig. 5(a). This is primarily because a higher current produces a higher gas temperature and, hence, a higher exit velocity of the plasma gas. A similar reasoning is applicable to the small increase of temperature of ZrO_2 particles with the current (Fig. 5b). But this effect is weaker in the case of NiCrAlY temperature, since the temperature has already become close to its boiling point, which is the maximum the particle can attain.

4.4 Particle Velocity and Temperature with the Variation of H_2 Flow Rate

The effect of hydrogen flow rate on the velocity and temperature of particles is displayed in Fig. 6. The calculation results, again in good agreement with the experimental data, reveal the general trend of the effect of the hydrogen flow rate. This trend for the particle velocity is easy to understand and is consistent with the increase of plasma velocity with the hydrogen flow rate, as shown in Fig. 2. However, the fact that a lower plasma temperature is obtained at a higher hydrogen flow rate, as well as that the residence time of an in-flight particle becomes shorter at a higher flow rate, seems to suggest that particle temperature may be lower at a higher hydrogen flow rate. This is contradictory to what we observed in Fig. 6(b). An increase in particle temperature with the hydrogen flow rate can be attributed to the higher thermal conductivity of the plasma mixture because of the increase in the hydrogen content.

The increase in particle velocity and temperature is especially strong when the flow rate increases from zero to about 4 slm, as seen in Fig. 6(a). This result suggests an optimum in the flow rate of hydrogen, about 4 slm for a given set of parameters, above which the benefit of an increase in hydrogen flow rate diminishes.

4.5 Species Segregation and Optimization of Spray Conditions

The deposition position of a particle is determined by its trajectory, which in turn depends largely on the injection conditions. In the calculations we present below, two different powder injection configurations are used. One is the mixed injection. Both metal and ceramic powders are injected through one injector. The position of the injector is the same as in the case discussed above and shown in Fig. 1.[1] Both kinds of powder particles have the same injection velocity, 11.7 m/s, as listed in Table 4. Another injection configuration considered here assumes that the metal and ceramic powders are injected from two separate injectors. The position of the injector for ZrO_2 is the same as displayed in Fig. 1. The injector for NiCrAlY is, however, located at an axial distance of 10 mm, 4 mm downstream from the ceramic injector. This arrangement of injectors considers that the NiCrAlY particles traverse a little further than ZrO_2 in the direction of injection, as well as the fact that NiCrAlY can be more easily melted. The injection velocity for each powder is listed in Table 4.

One Injector, Mixed Injection Figure 7(a) shows the approximate deposition areas of ZrO_2 and NiCrAlY materials under the mixed injection conditions. The coordinates used in the plot indicate the vertical direction (powder injection direction) and horizontal direction (vertical to the plane formed by plasma jet and powder injection direction). As shown in this plot, most NiCrAlY particles deposit a few millimeters below the ZrO_2 particles. This result roughly repeats the observation made by Jewett *et al.*[3] (In their observation, they found that the metal was concentrated in the lower right of the deposit and the ce-

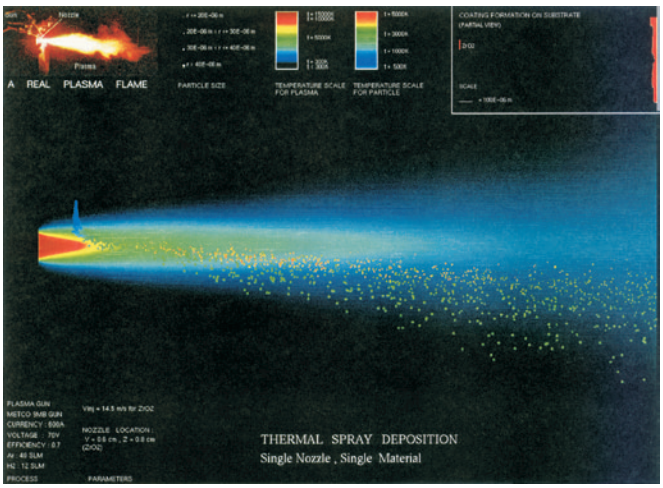

Fig. 8 Visualized temperature field of plasma jet with particle trajectories and temperatures. Particle sizes are also demonstrated by the size of the images. Particles shown here are PSZ particles

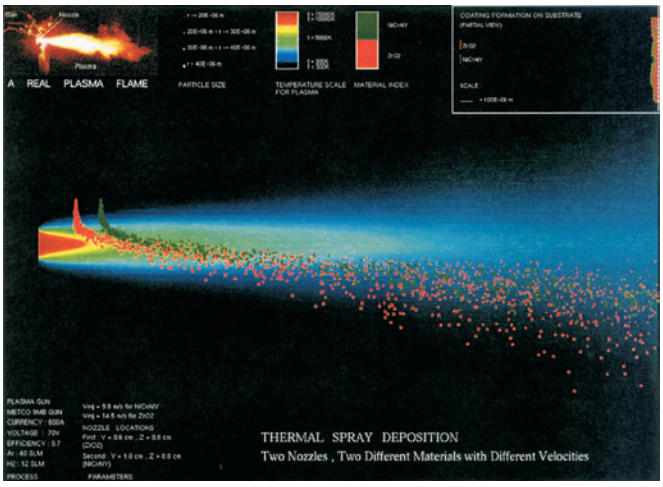

Fig. 10 Two injectors are used for two different powders. Injection velocity for PSZ is 14.5 m/s, much higher than that for NiCrAlY (9.8 m/s

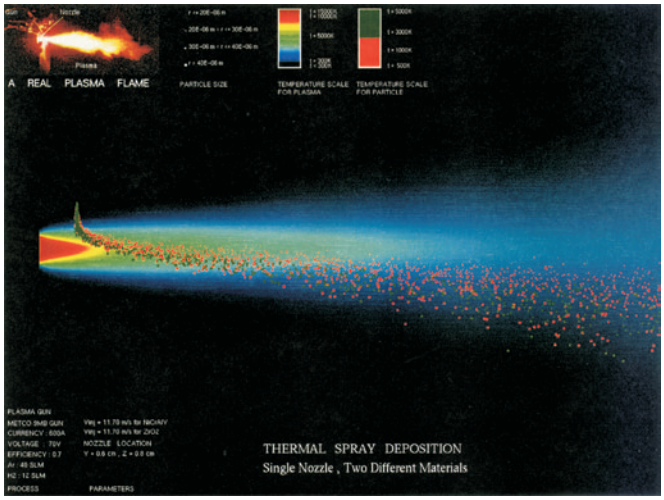

Fig. 9 Different colors of particles represents two different materials. Red refers to PSZ particles and green to NiCrAlY particles. Two kinds of powders injected mixed at the same time

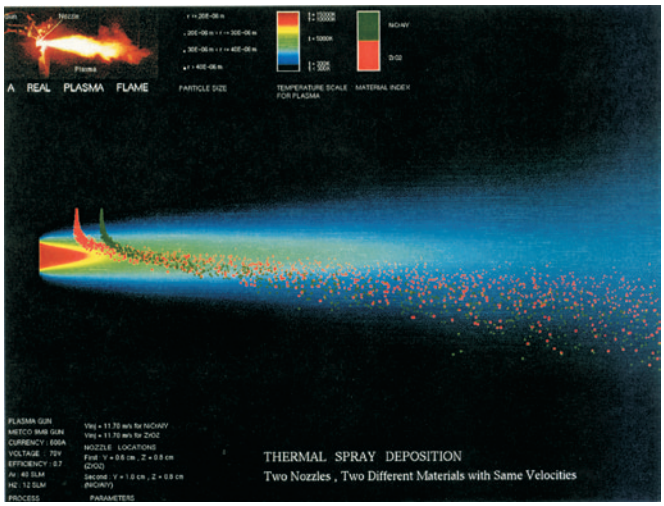

Fig. 11 Same injection velocity (11.7 m/s) for both powders is used to achieve better mixing of particles of different materials

ramic was segregated to the upper left. The slight shift in horizontal direction in experiments is due to the swirl of the plasma plume.)

The trajectories of different powders are visualized clearly in Fig. 9 by the circles with two different colors. Generally, NiCrAlY particles traverse a little further through the flame due to their higher density (or larger inertia). Therefore, the two kinds of powder materials are segregated during their flight in the gas flame and produce lower homogeneity in the coating. Furthermore, since NiCrAlY has much lower melting and boiling points than PSZ, it may be vaporized significantly while PSZ is just around or below its melting point.

Two Injectors, Different Injection Velocity The segregation of different species needs to be avoided in the spraying of FGMs. Using two separate injectors, as we mentioned before, is one of the many possibilities. Figure 10 shows an effort in this direction. The injector for NiCrAlY is moved a little bit downstream with the consideration that NiCrAlY is heavier and easier to be melted. The injection velocity for these two materials needs to be optimized for the purpose of good mixing of two component particles. If the injection velocities selected for NiCrAlY and PSZ are 9.8 and 14.5 m/s, respectively, as in the case of a single injector, separate injection (Table 4 and Fig. 8), the resulting spray still has a segregated pattern at the standoff of 100 mm (the maximum axial distance shown in figures is 150 mm), as shown in Fig. 10. The PSZ particles are further traversed through the flame because of their higher injection velocity and a little more travel distance. This suggests that the injection velocity of NiCrAlY should be increased and that of PSZ should be decreased.

Two Injectors, Same Injection Velocity An improvement on the mixing of the in-flight NiCrAlY and PSZ particles at 100

mm standoff is obtained by using the same injection velocity (11.7 m/s) for both materials, as shown in Fig. 11. From the deposition position shown in Fig. 7(b), the overlap of the deposition areas of the two powder materials is improved by using such an arrangement. This benefit comes from the fact that the position of the injector for NiCrAlY is away from the gun nozzle, which results in less distance traveled by the heavy metal particles. It demonstrates that, with the help of simulation and visualization, an optimized injection velocity can be obtained easily and effectively.

It needs to be pointed out that, in the configuration of two injectors, the upstream injector may have strong influence on the flow field near the downstream injector and, hence, on the behavior of the particles injected through the second injector. However, our calculations currently ignore the effect of carrier gas; this influence needs to be examined further.

5. Conclusions

Calculations are performed for plasma spray coating of PSZ and NiCrAlY alloy as functionally graded materials. Several plasma-operating conditions are considered to examine the effects of arc currency, voltage, and hydrogen flow rate. The predicted particle temperature and velocity conditions are compared with the measurements carried out at INEEL. The agreement between the calculations and the experiments clearly demonstrates the capability of the computational code, LAVA-P, in simulating the particle behavior when they pass through the plasma. Results on the particle velocity and temperature show that the particles with smaller sizes traverse less in the powder injection direction, along the plasma central axis, and they usually have higher velocities and temperatures than the larger one. Most of the ZrO_2 particles larger than 80 μm can not be fully melted even under the favorable heating conditions. The effect of current and hydrogen flow rate on the velocity and temperature of particles has also been analyzed. Higher values of power current and hydrogen flow rate usually result in higher particle velocity and temperature. The high-density materials move away from the central axis and further through the plasma plume. As a result, the difference in density of the components in FGMs causes the segregation of species affecting the uniformity and consistency of the deposition. The segregation can be greatly reduced and controlled by using a separate injector for each powder material and rearranging their locations as well as the velocity of particles in each injector. The LAVA-P code, together with a visualization algorithm, is an effective tool for the optimization of FGM coatings.

Acknowledgments

Acknowledgments are extended to the National Science Foundation (MRSEC Program under Award No. DMR-9632570) and the Idaho National Engineering and Environment Laboratory, University Research Consortium Program, managed by Lockheed Martin Corporation for the U.S. Department of Energy.

References

1. W.D. Swank, J.R. Fincke, D.C. Haggard, S. Sampath, and W. Smith: in *Thermal Spray: A United Forum for Scientific and Technological Advances*, C.C. Berndt, ed., ASM International, Materials Park, OH, 1997, pp. 451-58.
2. W. Smith, T.J. Jewett, S. Sampath, W.D. Swank, and J.R. Fincke: in *Thermal Spray: A United Forum for Scientific and Technological Advances*, C.C. Berndt, ed., ASM International, Materials Park, OH, 1997, pp. 599-605.
3. T.J. Jewett, W.C. Smith, H. Herman, J. Margolies, and S. Sampath: in *Thermal Spray: A United Forum for Scientific and Technological Advances*, C.C. Berndt, ed., ASM International, Materials Park, OH, 1997, pp. 607-12.
4. Y.P. Wan, V. Prasad, G.-X. Wang, S. Sampath, and J.R. Fincke: *J. Heat Transfer*, 1999, vol. 121, pp. 691-99.
5. J.D. Ramshaw and C.H. Chang: *Plasma Chem. Plasma Processing*, 1993, vol. 12 (3), pp. 299-325.
6. J.D. Ramshaw and C.H. Chang: J. Comput. Phy., 1995, vol.116, pp. 359-64.
7. C.H. Chang and J.D. Ramshaw: *Plasma Chem. Plasma Processing (Suppl.)*, 1996, vol. 16 (1), pp. 5S-17S.
8. B.E. Launder and D.B. Spalding: *Mathematical Models of Turbulence*, Academic Press, New York, NY, 1972.
9. Y.C. Lee, K.C. Hsu, and E. Pfender: *Proc. 5th Int. Symp. on Plasma Chemistry*, 1981, vol. 2, p. 795.
10. X. Chen and E. Pfender: *Plasma Chem. Plasma Processing*, 1983, vol. 3 (1), pp. 97-112.
11. Y.P. Wan, V. Gupta, H. Zhang, A. Varshney, S. Sampath, V. Prasad, and J.R. Fincke: *Proc. ASME*, ASME, Philadelphia, PA, 1999, HTD-vol. 364-3, pp. 389-94.
12. G.V. Samsonov: *The Oxide Handbook*, Plenum Press, New York, NY, 1973 (translated from Russian).
13. R. Hultgren, P.D. Desai, D.T. Hawkins, M. Gleiser, K.K. Kelley, and D.D. Wagman: *Selected Values of the Thermodynamics Properties of the Elements*, ASM, Metals Park, OH, 1973, pp. 350-57.